Photophysics of PAMAM-Based Dendrimers of Polypyridyl Complexes of Ruthenium

Samantha Glazier, Jason A. Barron, Paul L. Houston,* and Héctor D. Abruña*

Department of Chemistry and Chemical Biology, Baker Laboratory, Cornell University, Ithaca, New York 14853-1301

Received: August 27, 2001; In Final Form: July 9, 2002

The photophysics of PAMAM (poly-amidoamine) based dendrimers (generations G0-G4) modified with (4, 8, 16, 32, and 64) pendant-$[Ru(tpy)_2]^{+2}$ (tpy is 2,2′:6′,2″-terpyridine) and $[Ru(bpy)_3]^{+2}$ (bpy is 2,2′-bipyridine) chromophores have been studied in both fluid solution at 298 K and frozen glasses, at 77 K. The absorption and emission spectra, the excited-state lifetimes and quantum yields have been obtained for both families of metallodendrimers. In general and in analogy to the behavior exhibited by the discrete molecules (i.e., $[Ru(tpy)_2]^{+2}$ and $[Ru(bpy)_3]^{+2}$), the bipyridine derivatives exhibit longer lifetimes and higher quantum yields when compared to the corresponding terpyridine complexes. Some generation dependent changes have also been observed. We have also explored the effects of solvent by comparing results in butyronitrile and dimethylacetamide with the latter being used as a mimic of the dendritic backbone. Our results suggest that for the higher generations the dendritic backbone acts as the solvent in affecting the photophysical behavior.

Introduction

The study of the photochemistry and photophysics of polypyridyl complexes of ruthenium has been an area of research that has received a great deal of attention for over 25 years. Particular interest has been placed in the study of the 2,2′-bipyridine and 2,2′:6′,2″-terpyridine complexes as well as their derivatives.[1−6] This interest derives, in part, from a desire to obtain a detailed understanding of the rich photochemistry and photophysics that these materials exhibit. In addition, their potential utility in solar energy conversion schemes served as an additional impetus.[7] As a result, a vast number of such complexes have been synthesized and characterized.[8]

Of more recent interest has been the synthesis and characterization of supramolecular systems for use in performing complex molecular functions.[9−11] Broad families of materials have been prepared and characterized, including coordinated networks, catenananes, rotoxanes, and dendrimers.[12,13]

Dendrimers are highly branched molecules that can be synthesized in well-defined patterns and sizes (generations) that allow control over molecular weight, topology, cavity size, and surface functionality.[14−22] There has been a great deal of effort in the synthesis and characterization of variously modified dendrimers because of the numerous potential applications that such materials present. Similarly, there has also been a great deal of interest in the study of the adsorption of dendrimers onto different types of surfaces for applications in molecular recognition and in the deliberate design of functional coatings and smart interfaces. An understanding of the factors controlling the interaction of dendrimers with surfaces, including size (generation) and functional groups present, would be of great value in tailoring modified surfaces for specific applications. Of particular interest are dendrimers with electroactive and/or photoactive centers, because one could use the electrode potential or light as an additional stimulus for controlling and/or modulating interactions. These interactions could, in turn, give rise to the formation of tailored surface structures.

We have synthesized and characterized a variety (generations 0−4 with 4, 8, 16, 32, and 64 groups on the periphery, respectively) of polyamidoamine (PAMAM) dendrimers (Figure 1) containing pendant bipyridine or terpyridine ligands onto which Ru, Fe, Co, Re, as well as numerous other transition metal complexes may be attached through coordination. These materials are synthesized from the PAMAM starburst dendrimers to yield the ligand containing species that are subsequently reacted to yield the transition metal complex derivatized species. The interest in these materials was stimulated not only by their redox chemistry but also by their photochemical reactivity. In this regard, the study of dendrimers containing pendant $[Ru(tpy)_2]^{+2}$ or $[Ru(bpy)_3]^{+2}$ chromophores is of particular interest.

In previous work, we carried out a preliminary characterization of the absorption and emission spectra of dendrimers with pendant $[Ru(tpy)_2]^{+2}$ or $[Ru(bpy)_3]^{+2}$ groups.[23] However, the influence of the supramolecular system on the photophysical properties was not explored in those studies. Through the use of time correlated single photon counting (TCSPC) experiments, we have now been able to examine the luminescence lifetimes of these dendritic materials with pendant $[Ru(tpy)_2]^{+2}$ or $[Ru(bpy)_3]^{+2}$ chromophores at room (298 K) and low (77 K) temperature and to assess the influence of the supramolecular architecture on the photophysical behavior. We have also explored solvent effects by comparing the photophysical behavior of these materials in acetonitrile, butyronitrile, and dimethyacetamide (DMAA), with the latter serving as a mimic of the dendritic backbone.

Experimental Section

Materials. $[Ru(tpy)_2]$-PAMAM dendrimers (dend-n-$Ru(tpy)_2$ n = 4, 8, 16, 32, 64) and $[Ru(bpy)_3]$-PAMAM dendrimers (dend-n-$Ru(bpy)_3$ n = 4, 8, 16, 32, 64) were obtained from previous work.[23] The dendrimers were purified by dichloromethane/ether recrystallization and purity was confirmed by thin-layer chromatography, NMR, elemental analysis, and mass spectrometry.

* To whom correspondence should be addressed.

10.1021/jp013312c CCC: $22.00 © 2002 American Chemical Society
Published on Web 09/10/2002

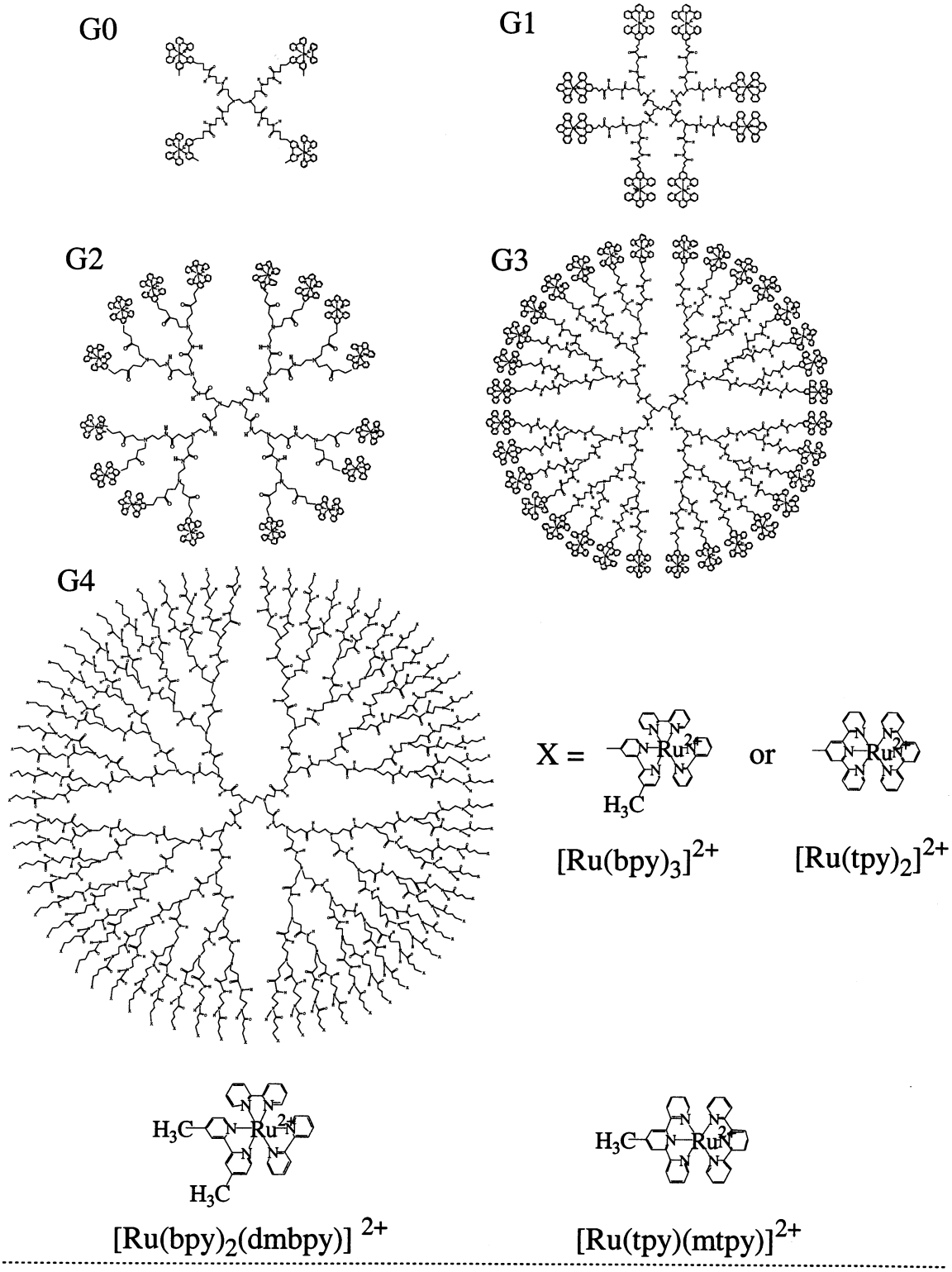

Figure 1. Structure of five generations (G#) of ruthenium PAMAM dendrimers and the model compounds $[Ru(bpy)_2(dmbpy)]^{2+}$ and $[Ru(tpy)(mtpy)]^{2+}$.

$[Ru(tpy)(mtpy)]^{2+}(PF_6)_2$ (mtpy is 4′-methyl-2,2′:6′,2″-terpyridine) was synthesized by reacting $[Ru(tpy)(Cl_3)]$ with a 1:1 molar ratio of mtpy in refluxing ethanol. The reaction mixture was allowed to cool, and the complex was precipitated by the addition of a solution of NH_4PF_6 in water. The complex was collected, rinsed with water and ether, and purified by a second precipitation from acetonitrile with ether.

$[Ru(bpy)_2(dmbpy)]^{2+}(PF_6)_2$ (dmbpy is 4,4,′-dimethyl-2,2′-bipyridine) was synthesized by reacting $[Ru(bpy)_2Cl_2]$ with a molar excess of dmbpy in refluxing ethanol/water. The complex was isolated and purified as described above for $[Ru(tpy)(mtpy)]^{2+}(PF_6)_2$.

Acetonitrile was purchased from Burdick and Jackson and dried over 4 Å molecular sieves. Butyronitrile was purchased from Aldrich (98%), fractionally distilled, and dried over molecular sieves. Glassware was cleaned via a chromerge bath and washed and rinsed in Millipore ultrapure water with a resistivity greater than 18 MΩ. Fluorescence cuvettes were

TABLE 1: Summary of Photophysical Data for All Compounds at 77 and 298 K

	emission max. (nm)[b]			τ (μs)[b]			ϕ[b,c]	
compound	298 K	DMAA	77 K	298 K	DMAA[d]	77 K	298 K	77 K
$[Ru(tpy)_2]^{2+}$	615	620	603.5	125×10^{-6}	235×10^{-6}	11.1	(1.0×10^{-6})	(0.48)
$[Ru(tpy)(mtpy)]^{2+}$	625	625	605.0	85×10^{-6}	170×10^{-6}	10.1		0.25
dend-4-$Ru(tpy)_2$	625	625	606.0	95×10^{-6}	175×10^{-6}	9.70		0.25
dend-8-$Ru(tpy)_2$	625	625	610.0	95×10^{-6}	190×10^{-6}	9.52		0.23
dend-16-$Ru(tpy)_2$	625	625	610.2	115×10^{-6}	180×10^{-6}	8.54		0.22
dend-32-$Ru(tpy)_2$	625	625	610.7	120×10^{-6}	210×10^{-6}	8.10		0.19
dend-64-$Ru(tpy)_2$	625	625	611.0	140×10^{-6}	210×10^{-6}	6.72		0.22
$[Ru(bpy)_3]^{2+}$	606.0	608.0	585.0	0.95	0.620	5.95	(0.066)	(0.40)
$[Ru(bpy)_2(dmbpy)]^{2+}$	612.0	614.0	586.5	1.05	0.475	5.50	0.049	0.25
dend-4-$Ru(bpy)_3$	614.5	620.0	593.9	1.05	0.905	5.50	0.049	0.29
dend-8-$Ru(bpy)_3$	616.0	620.0	594.0	1.00	0.750	5.45	0.024	0.14
dend-16-$Ru(bpy)_3$	617.0	620.0	595.5	0.65	0.540	4.40	0.021	0.12
dend-32-$Ru(bpy)_3$	617.5	620.0	595.0	0.65	0.465	4.20	0.021	0.12
dend-64-$Ru(bpy)_3$	617.5	620.0	597.5	0.70	0.505	4.70	0.042	0.48

[a] All of the $[Ru(bpy)_3]^{2+}$ complexes are in butyronitrile at 77 and 298 K. [b] Error for λ_{em} values are 0.5%. Error in τ and ϕ_{298K} are 5%. Error in ϕ_{77K} values are 10%. [c] () indicates that the value is a literature value. See text for references. [d] 298 K.

cleaned with "piranha" solution. (4:1 concentrated sulfuric acid: 30% hydrogen peroxide; **Caution: This solution reacts violently with organics!**). The concentrations of the dendrimers and model compounds were between 10 and 0.6 μM and made with particular emphasis placed on keeping the metal complex concentrations similar in all generations. Samples for room-temperature luminescence studies were degassed for over 20 min before study.

Room-temperature samples were measured in quartz cuvettes using acetonitrile as solvent for the $[Ru(tpy)_2]^{2+}$ complexes and butyronitrile for the $[Ru(bpy)_3]^{2+}$ complexes. Low-temperature samples were measured in NMR tubes using butyronitrile: absolute ethanol (9:1) as the solvent for the $[Ru(tpy)_2]^{2+}$ pendant complexes and butyronitrile for $[Ru(bpy)_3]^{2+}$ pendant complexes. These allowed for clear stable glasses that were fairly resistant to cracking even when exposed to peak laser powers greater than 2 kW. The stability of the glasses decreased with the absorption of water by the butyronitrile solvent. Water contamination caused "fogging" or cracking of the glass. Samples were placed in a clear glass dewar containing liquid nitrogen.

Apparatus

Picosecond Lifetime Measurements. Room-temperature experiments of $[Ru(tpy)_2]^{2+}$ pendant dendrimers and model complexes were carried out using a time correlated single photon counting system (TCSPC) which consisted of a mode-locked Spectra Physics Tsunami Ti:sapphire laser (82 MHz repetition rate) which was pumped by a Spectra Physics argon ion laser (10 W). Pulses were less than 100 fs fwhm, and the bandwidth was monitored via an Ist-Rees laser spectral analyzer during the experiment. Laser light was doubled in a β-Barium Borate crystal to provide excitation wavelengths from 380 to 420 nm. The final excitation power generated was approximately 20 mW. The beam was filtered and focused onto a 1 cm^2 fluorescence cell, and the output was collected at 90°. The fluorescence was collimated with a 2″ collection lens (2″ focal length), filtered, and focused into a single monochromator (2.5 mm slits). The signal was collected with a Hamamatsu PMT-MCP (R1564−07) cooled to −20 °C. It was then amplified using an EG&G Ortec 9306 1 GHz preamp and fed into a Becker and Hickl SPC-300 computer module. This module contains the constant fraction discriminator, analogue to digital converter, and time to amplitude converter. It uses a reversed start−stop system to provide 13 ps time resolution and repetition rates of 200 MHz. The start pulse was obtained by focusing a reflection of the fundamental beam onto a Becker and Hickl PHD-400-N photodiode. The start pulses were monitored with a Lecroy digital oscilloscope. Room-temperature data were deconvolved and fit through the use of the SPCFit program provided by Dr. Ahmed Heikel.

Nanosecond Lifetime Measurements. Low-temperature experiments were carried out using a Lambda Physik LPX-205i Excimer laser at 308 nm and 10 Hz, pumping a Lambda Physik dye laser using Coumarin 450 laser dye to provide 500 μJ of light at 460 nm. Pulses were 20 ns fwhm. Samples were cooled in glass NMR tubes in liquid nitrogen and then placed in a glass dewar, and the fluorescence was collected at 90°. A 2″ collection lens was used in conjunction with a focusing lens and several filters (OG570, RG590, and RG610) to bring the fluorescence through a single monochromator (Bausch & Lomb) equipped with a PMT (Hamamatsu E990-07). Data were collected on a Lecroy digital oscilloscope, converted into ASCII format, and analyzed with Origin (Microcal, Inc.) computer software.

Spectrofluorimeter. Fluorescence spectra were obtained using a SPEX 1681 Minimate-2 spectrofluorimeter with a Spectra Acq CPU controller. All spectra were acquired at 90° relative to the incident beam. Quantum yields were calculated using the known quantum yields of either $[Ru(tpy)_2]^{2+}$ ($\Phi_{77K} = 0.48$, $\Phi_{298K} = 1 \times 10^{-6}$) or $[Ru(bpy)_3]^{2+}$ ($\Phi_{77K} = 0.40$, $\Phi_{298K} = 0.066$).[8]

UV−Visible Absorption. UV−visible data were obtained using a HP 8453 diode array spectrometer. Spectra were obtained in quartz cuvettes at room temperature.

Results

Emission Spectra. *Low-Temperature Spectra.* Normalized emission spectra for dend-n-$Ru(tpy)_2$ (n=8 and 64), $[Ru(tpy)_2]^{+2}$, and $[Ru(tpy)(mtpy)]^{2+}$ (the latter two used as reference "model compounds") were obtained at 77 K, and the data are summarized in Table 1. The principal emission peak of $[Ru(tpy)_2]^{+2}$ is centered at 603.5 nm (16 570 cm^{-1}). Initial excitation is to a singlet metal-to-ligand charge transfer (MLCT) state that decays nonradiatively to a nearby triplet MLCT state. The probability of this transition is assumed to be equal to 1 with a lifetime of ~1 ps.[8] The excited electron in the MLCT state is localized on a single ligand.[24] The principal peak in the emission spectrum corresponds to the subsequent radiative transition from the triplet MCLT state to the lowest vibrational level in the ground electronic state. A shoulder at 650 nm (15 385 cm^{-1})

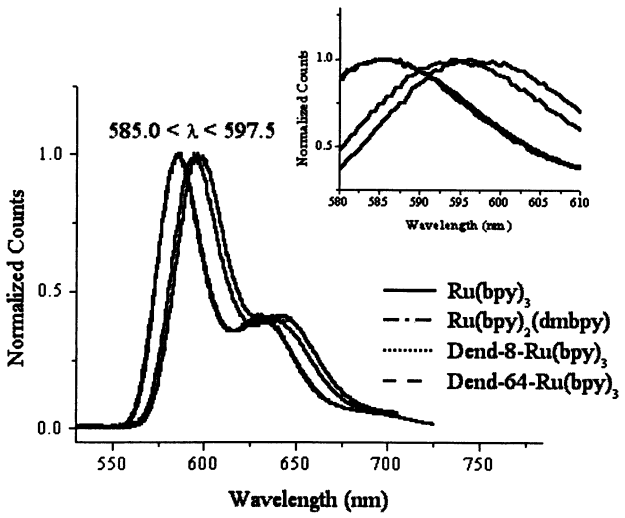

Figure 2. Normalized emission spectra for dend-*n*-Ru(bpy)$_3$ (n = 8 and 64), $[Ru(bpy)_3]^{+2}$, and $[Ru(bpy)_2(dmbpy)]^{2+}$ at 77 K. Inset shows the red shift in the peak maximum with increasing dendrimer generation.

in the spectrum is ascribed to emission to a higher vibrational level in the ground electronic state with 1185 cm^{-1} less energy.[25]

Because in the dendritic materials one of the terpyridines within the metal complex is bound to the organic backbone at the 4′-position, $[Ru(tpy)(mtpy)]^{2+}$ was considered to be a more appropriate model compound. Although the emission properties of this complex were, as would be anticipated, very similar to those of $[Ru(tpy)_2]^{+2}$, there was a 1.5 nm (41 cm^{-1}) shift in the emission maxima.

The spectra of dend-*n*-Ru(tpy)$_2$ (n = 8 and 64) showed a red shift in the principal emission peak with increasing dendrimer generation. Generation 0, with four $[Ru(tpy)_2]^{+2}$ chromophores, is red-shifted 2.5 nm to 606 nm (16 502 cm^{-1}), and generation 1 (with eight chromophores) shifted an additional 4 nm to 610.0 nm (16 393 cm^{-1}). Generations 2−4 exhibited maxima that were only slightly red-shifted with increasing generation and were centered around 611 nm (16 367 cm^{-1}).

Normalized emission spectra for dend-*n*-Ru(bpy)$_3$ (n = 8 and 64), $[Ru(bpy)_3]^{+2}$ and $[Ru(bpy)_2(dmbpy)]^{2+}$ at 77 K are shown in Figure 2. The excited-state manifold for $[Ru(bpy)_3]^{+2}$ complexes is structured identically to that described above for $[Ru(tpy)_2]^{+2}$ complexes and differs only in the positions of the energy levels. The principal emission peak of $[Ru(bpy)_3]^{+2}$, centered at 585.0 nm (17 094 cm^{-1}), is blue-shifted by 18 nm relative to $[Ru(tpy)_2]^{+2}$. For the same reasons described above for the $[Ru(tpy)_2]$-pendant dendrimers, $[Ru(bpy)_2(dmbpy)]^{2+}$ was considered to be a more appropriate model complex. Its principal emission peak is centered at 586.5 nm (17 050 cm^{-1}).

A comparatively large red shift, relative to $[Ru(bpy)_2(dmbpy)]^{2+}$, of the principal emission peak of dend-4-Ru(bpy)$_3$ to 593.9 nm (16 838 cm^{-1}) was observed. Incremental red shifts were observed for the other four dendrimer generations. These can be more clearly distinguished in the inset of Figure 2. Values for all of the emission wavelengths are presented in Table 1.

Room-Temperature Spectra. Normalized emission spectra for dend-*n*-Ru(bpy)$_3$ (n = 8 and 64), $[Ru(bpy)_3]^{+2}$, and $[Ru(bpy)_2(dmbpy)]^{2+}$ at 298 K were obtained, and the data are summarized in Table 1. The principal emission peak of $[Ru(bpy)_3]^{+2}$ is centered at 606.0 nm (16 502 cm^{-1}) and 612.0 nm (16 340 cm^{-1}) for $[Ru(bpy)_2(dmbpy)]^{2+}$. For the dendrimers, a slight red shift is observed with increasing generation, but the large shift observed at 77 K between $[Ru(bpy)_2(dmbpy)]^{2+}$and dend-4-Ru(bpy)$_3$ is not present at 298 K. For the dend-*n*-Ru(bpy)$_3$ (n = 4, 8, 16, 32, and 64), we observed a small but quantifiable red shift from 614.5 nm (16 273 cm^{-1}) for G0 to 617.5 nm (16 194 cm^{-1}) for G4. The emission energies of G0-G1 and G2-G4 are closely matched within each series with a 2 nm (52 cm^{-1}) difference between the two series. Values for all of the emission wavelengths are presented in Table 1. This pattern parallels the structural differences between G0-G1 and G3-G4. We have previously shown that there are generation-dependent variations in the structure.[26] Specifically, the lower generations (G = 0 and 1) have relatively open structures, whereas the higher generations (G = 3 and 4) are much more compact and globular.

The room-temperature emission from dend-*n*-Ru(tpy)$_2$ is centered around 625 nm (16 000 cm^{-1}). The very weak emission at 298 K for these chromophores precluded a precise determination of small changes in the position of the principal peak maximum.

Solvent Dependence. Polypyridine complexes of ruthenium are known to exhibit solvent dependent emission.[8,27−30] Given the structural differences discussed above, we thought that there would be concomitant differences in the extent of solvation of the individual chromophores, with lower generations having a solvation sphere around the chromophores that was dominated by the solvent in which the dendrimers were dissolved. For the larger generations, we thought that the dendritic backbone/branches would play a significant role, possibly acting as a solvent. [See the Appendix for additional discussion on the changes in solvent sphere with generation.] One of the conclusions from a recent study of the kinetics of interfacial charge transfer for adsorbed dend-64-$[Ru(tpy)_2]$ on platinum microelectrodes was that the dendritic branches did, indeed, appear to strongly influence, if not dominate, the solvation of the individual $[Ru(tpy)_2]^{+2}$ units.[31,32] In addition, Stephens et al. measured the photophysical properties of $[Re(bpy)(CO)_3NC(CH_2)_nCH_3]^+$, n = 0−17, and found that the emission peak maxima and lifetimes strongly depended on n which was a result of the ability of the alkly chain to fold back on itself thus altering the solvent sphere around the excited portion of the molecule.[33] In an effort to assess such solvent effects, spectra were obtained in dimethylacetamide (DMAA). This solvent was chosen because it served as a small molecule mimic of the dendritic branches.

Even with the limitations of a low quantum yield at 298 K for $[Ru(tpy)_2]^{+2}$ compounds, there was a change in the emission maximum of 5 nm from 615 nm (16 260 cm^{-1}) in butyronitrile to 620 nm (16 129 cm^{-1}) in DMAA for $[Ru(tpy)_2]^{+2}$. For the dend-*n*-Ru(tpy)$_2$ dendrimers, the same peak maxima were observed in both solvents. The red shift of the peak maximum of the discrete molecule $[Ru(tpy)_2]^{+2}$, used as a model compound, in DMAA and the constant peak position of the dend-*n*-Ru(tpy)$_2$ dendrimers in both solvents would suggest that the dendrimer arm has a similar effect on the energy of the emitting state as using DMAA as the solvent. In essence, both lower the energy of the emitting state by approximately 200 cm^{-1}. Values of the emission wavelengths in DMAA are presented in Table 1. The higher quantum yield of the $[Ru(bpy)_3]^{+2}$ complexes allowed us to examine solvent effects in more detail.

For all $[Ru(bpy)_3]^{+2}$ complexes in DMAA, red shifts, relative to butyronitrile, of approximately 3 nm (81 cm^{-1}) were measured. This trend is in agreement with the approximately 3 nm red shift between G0 and G4 in butyronitrile, again indicating that the dendrimer's branches and solvation by DMAA induce a small red shift in the emission peak maximum suggesting that the dendrimer backbone may be altering the

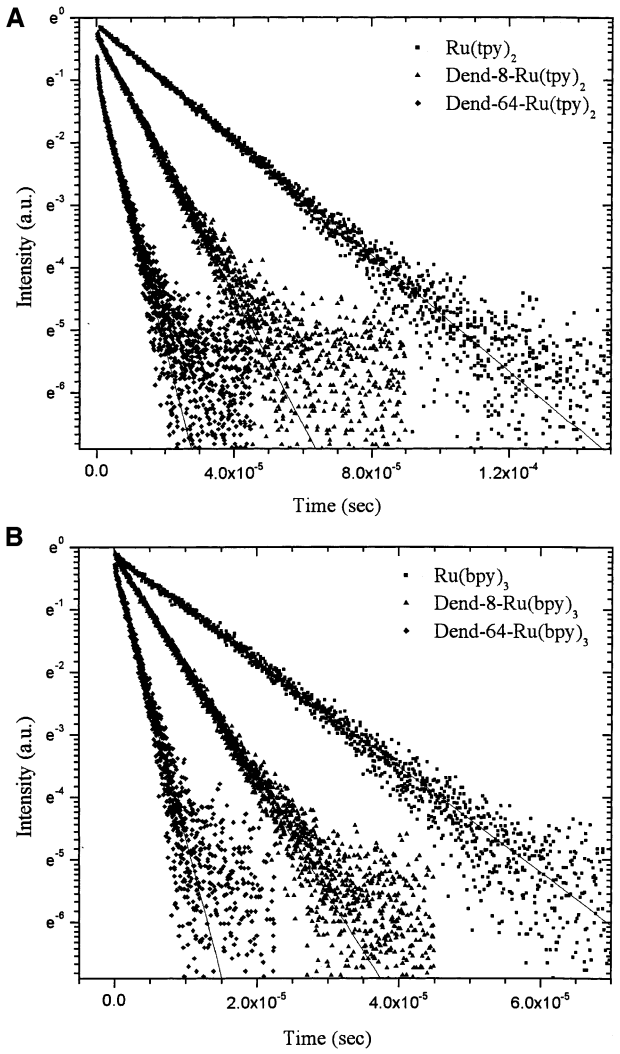

Figure 3. Luminescence decay profiles at 77 K for (A) $[Ru(tpy)(mtpy)]^{2+}$ and dend-*n*-$Ru(tpy)_2$ ($n = 8$ and 64) dendrimers and (B) $[Ru(bpy)_2(dmbpy)]^{2+}$ and dend-*n*-$Ru(bpy)_3$ ($n = 8$ and 64) dendrimers. For clarity, the *x* scale has been multiplied a factor of 0.5 for $[Ru(tpy)(mtpy)]^{2+}$ and $[Ru(bpy)_2(dmbpy)]^{2+}$, a factor of 1 for dend-8-Ru$(tpy)_2$ and dend-8-Ru$(bpy)_3$, and a factor of 2 for dend-64-Ru$(tpy)_2$ and dend-64-Ru$(bpy)_3$, respectively. The solid lines represent the best fit of the data to a single-exponential decay.

solvent sphere around the metal center. No changes in emission maxima between G0 and G4 were observed in DMAA. However, an unexpectedly large difference of 6 nm (158 cm^{-1}) between $[Ru(bpy)_2(dmbpy)]^{2+}$ and G0 in DMAA was measured. If solvation of the chromophore by the dendrimer branches was the only factor shifting the emission energy, then no difference in emission maxima would be expected for the model compounds and the dendrimers. The differences in coordination around the Ru metal centers arising from the differences in the ligands could give rise to shifts in the energy level of the emitting state thus accounting for the differences between the model compound and G0.

Time-Resolved Luminescence Spectra. *Low Temperature.* The luminescence lifetimes of $[Ru(tpy)(mtpy)]^{2+}$, $[Ru(tpy)_2]^{+2}$, and dend-*n*-$Ru(tpy)_2$ ($n = 4$, 8, 16, 32, and 64) were obtained at 77 K in 9:1 butyronitrile:ethanol. Figure 3A shows the decay profiles for dend-*n*-$Ru(tpy)_2$ ($n = 8$ and 64) as well as for the $[Ru(tpy)(mtpy)]^{2+}$ model compound. The decay profiles were each fit by a single exponential, and the luminescence lifetimes calculated from the fitting procedure are presented in Table 1.

SCHEME 1: Excited State Manifold of $[Ru(tpy)_2]^{2+}$. At Room Temperature, Enough Thermal Energy Is Available to Make the ^{3}MC State Accessible from the ^{3}MCLT State. The ^{3}MC State Decays Nonradiatively.

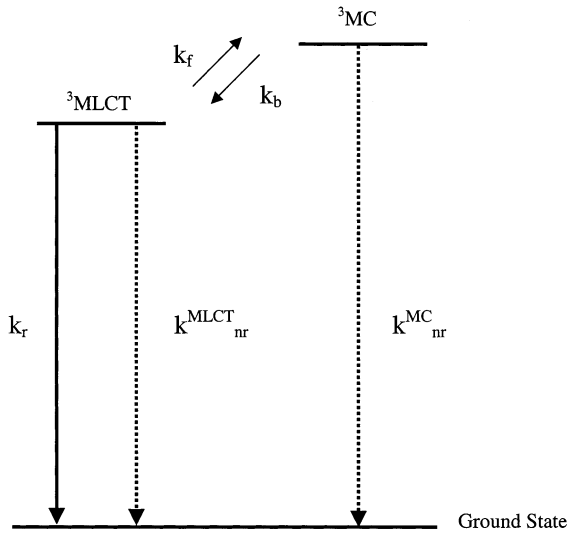

The lifetimes decreased monotonically from 11.1 μs for $[Ru(tpy)_2]^{+2}$ (10.1 μs for $[Ru(tpy)(mtpy)]^{2+}$) to 6.72 μs for dend-64-$Ru(tpy)_2$ corresponding to a 40% change (34% relative to $[Ru(tpy)(mtpy)]^{2+}$).

A similar set of experiments was carried out for $[Ru(bpy)_3]^{+2}$, $[Ru(bpy)_2(dmbpy)]^{2+}$, and dend-*n*-$Ru(bpy)_3$ in butyronitrile. Figure 3B presents the profiles for $[Ru(bpy)_2(dmbpy)]^{2+}$ and dend-*n*-$Ru(bpy)_3$ ($n = 8$ and 64). From the same type of analysis as described above, the luminescence lifetimes were calculated and are presented in Table 1. The monotonic decrease in the lifetime with increasing generation is similar to the generation dependence for the dend-*n*-$Ru(tpy)_2$ materials, with the exception of dend-64-$Ru(bpy)_3$, which exhibited an anomalously long lifetime. The trend in quantum yields also yielded an unexpected value in the case of dend-64-$Ru(bpy)_3$. The lifetime of dend-32-$Ru(bpy)_3$ was determined to be 4.22 μs, which was the shortest of all dendrimer generations measured at low temperature. In general, the change in lifetime with dendrimer generation was about half of that determined for dend-*n*-$Ru(tpy)_2$ materials at 77 K.

It should be noted that although there is a bit of scatter and noise at the tails of the profiles presented in Figure 3 parts A and B (as well as in those presented in Figures 4 and 5; vide-infra) it is clear that they are all well described by a single exponential.

Room Temperature. Because of the very short lifetimes of the $[Ru(tpy)_2]^{+2}$ complexes, a femtosecond laser system was employed, coupled with TCSPC detection, to compensate for the very low quantum yield of the emission process. For polypyridyl complexes of ruthenium, the conventional view is that terpyridine complexes, relative to the analogous bipyridine complexes, decay much faster because internal conversion to a nearby metal centered excited state (^{3}MC) is favored over radiative decay from the ligand centered (^{3}MLCT) because of a small separation between the two states. A diagram of the excited-state manifold at room temperature is presented in Scheme 1.

Normalized fluorescence decay profiles at room temperature and the corresponding fits for dend-*n*-$Ru(tpy)_2$ ($n = 4$, 16, and 64) are shown in Figure 4A, and the luminescence lifetimes obtained from the deconvolution and least-squares fitting

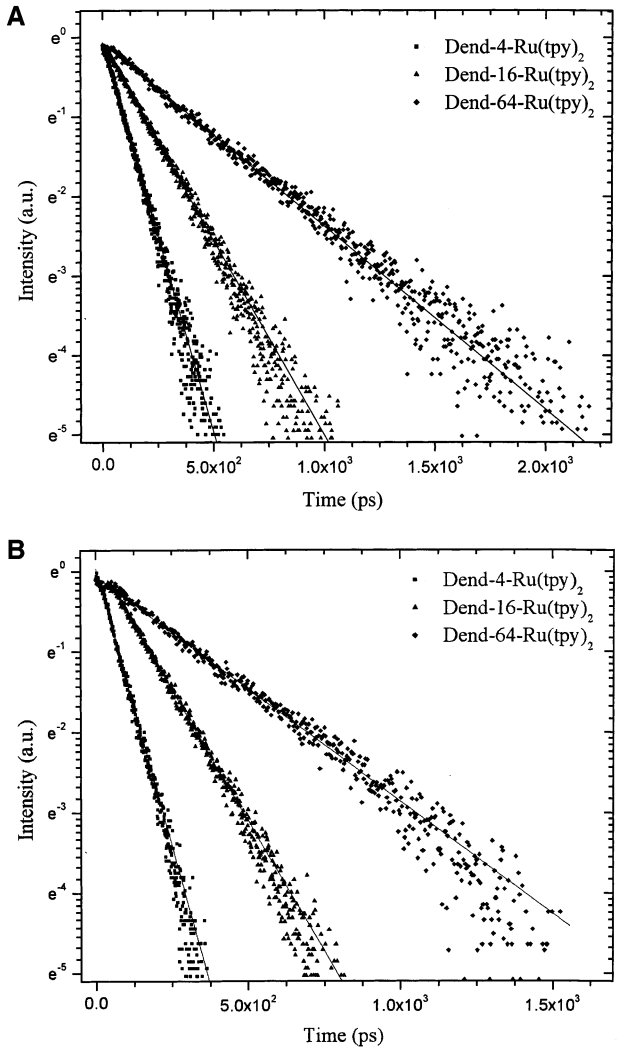

Figure 4. Luminescence decay profiles for dend-4-Ru(tpy)$_2$, dend-16-Ru(tpy)$_2$, and dend-64-Ru(tpy)$_2$ at 298 K in (A) DMAA and (B) acetonitrile. For clarity, the x scale has been multiplied a factor of 0.5 for dend-4-Ru(tpy)$_2$, a factor of 1 for dend-16-Ru(tpy)$_2$, and a factor of 2 for dend-64-Ru(tpy)$_2$, respectively. The solid lines represent the best fit of the data to a single-exponential decay.

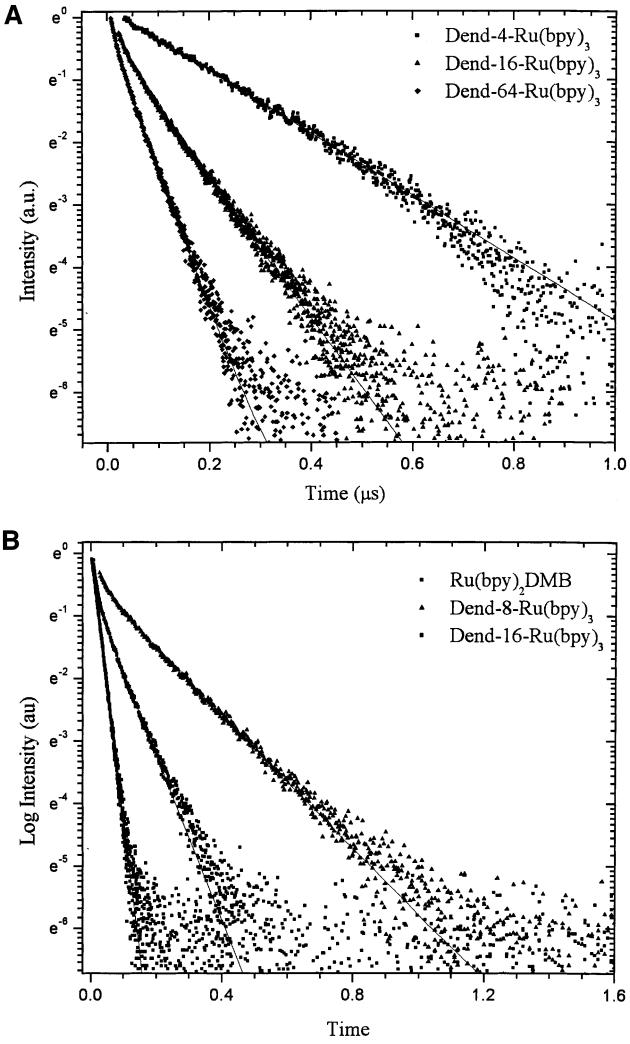

Figure 5. Luminescence decay profiles at 298 K for (A) dend-*n*-Ru(bpy)$_3$ (n = 4, 16, and 64) in butyrontrile and (B) for [Ru(bpy)$_2$(dmbpy)]$^{2+}$ and dend-*n*-Ru(bpy)$_3$ (n = 8 and 16) in DMAA. For clarity, the *x* scale has been multiplied a factor of 0.5 for dend-4-Ru(bpy)$_3$ and [Ru(bpy)$_2$(dmbpy)]$^{2+}$, a factor of 1 for dend-16-Ru(bpy)$_3$ (in butyronitrile) and dend-8-Ru(bpy)$_3$, and a factor of 2 for dend-64-Ru(bpy)$_3$ and dend-16-Ru(bpy)$_3$ (in DMAA), respectively. The solid lines represent the best fit of the data to a single-exponential decay.

analysis are presented in Table 1. The fluorescence lifetime for [Ru(tpy)(mtpy)]$^{2+}$ in acetonitrile was determined to be 88 ps, and the lifetimes for generations 0−4 increased monotonically from a value of 95 ps for dend-4-[Ru(tpy)$_2$] to 139 ps for dend-64-[Ru(tpy)$_2$], a change of 37%.

When DMAA was used as the solvent, the lifetimes of [Ru(tpy)(mtpy)]$^{2+}$, dend-4-Ru(tpy)$_2$, and dend-8-Ru(tpy)$_2$ were found to be approximately twice as long as in acetonitrile. This might reflect, at least to some extent, the difference in viscosity between the two solvents (η_{AN} = 0.345 cP; η_{DMA} = 0.92 cP) and suggests that nonradiative decay rate is a less efficient process in DMAA. Overall, the lifetimes increased with increasing dendrimer generation as for the acetonitrile case, but the overall change was less than 20%. Fluorescence decay profiles for dend-n-Ru(tpy)$_2$ (n = 4, 16, and 64) are presented in Figure 4B, and the values of the lifetimes are presented in Table 1. Inspection of the values reveals that when DMAA is used as the solvent the differences in lifetimes seen earlier when using butyronitrile are greatly attenuated. This observation supports the notion that the use of DMAA mimics the dendritic backbone, thus making the solvent sphere around each chromophore very similar and much less dependent on the generation of the dendrimer.

For [Ru(bpy)$_3$]$^{+2}$, [Ru(bpy)$_2$(dmbpy)]$^{2+}$, and dend-*n*-Ru(bpy)$_3$ the experimental setup employed was the same as that used at 77 K. The generation dependence was identical at both temperatures with the lifetimes decreasing with increasing generation, but not monotonically as observed at 77 K. Figure 5A shows the fluorescence decay profiles for dend-*n*-Ru(bpy)$_3$ (n = 4, 16, and 64) in butyronitrile. Values of the lifetimes are presented in Table 1. It can be noted that the lifetime values form two groups, G0-G1 and G2-G4, a behavior that again parallels the changes in structure with generation. The measurements were repeated using DMAA as the solvent (Figure 5B shows the profiles for [Ru(bpy)$_2$(dmbpy)]$^{2+}$ and dend-*n*-Ru(bpy)$_3$ n = 8 and 16), and the resulting emission lifetimes (Table 1) were shorter than in acetonitrile and had similar trends in terms of the generation dependence, though it was less pronounced. As in the previous case, there was a similar clustering of lifetimes as seen in butyronitrile, except there was a larger disparity between G0 and G1. Thus, we conclude that the solvent effects for the dend-*n*-Ru(bpy)$_3$ family are much less pronounced than for the corresponding dend-*n*-Ru(tpy)$_2$ materials.

TABLE 2: Radiative ($k_r = \phi/\tau$) and Nonradiative ($k_{nr} = 1/\tau - k_r$) Decay Rates for All Compounds at 77 and 298 K

	k_{nr}/s (k_r/s)		k_{nr}/s (k_r/s)		k_{nr}/s (k_r/s)	
compound	77 K[a]		298 K acetonitrile		298 K DMAA	
$[Ru(tpy)_2]^{2+}$	4.67×10^4	(4.31×10^4)	8.00×10^9	(0.800×10^4)	4.29×10^9	(0.429×10^4)
$[Ru(tpy)(mtpy)]^{2+}$	7.43×10^4	(2.48×10^4)	11.4×10^9	(0.568×10^4)	5.85×10^9	(0.292×10^4)
dend-4-$Ru(tpy)_2$	7.73×10^4	(2.58×10^4)	10.5×10^9	(0.526×10^4)	5.68×10^9	(0.284×10^4)
dend-8-$Ru(tpy)_2$	8.09×10^4	(2.42×10^4)	10.4×10^9	(0.521×10^4)	5.21×10^9	(0.260×10^4)
dend-16-$Ru(tpy)_2$	9.13×10^4	(2.58×10^4)	8.62×10^9	(0.431×10^4)	5.56×10^9	(0.278×10^4)
dend-32-$Ru(tpy)_2$	10.0×10^4	(2.35×10^4)	8.48×10^9	(0.424×10^4)	4.83×10^9	(0.242×10^4)
dend-64-$Ru(tpy)_2$	11.6×10^4	(3.27×10^4)	7.19×10^9	(0.360×10^4)	4.78×10^9	(0.239×10^4)
compound	77 K[b]		298 K butyronitrile		298 K DMAA	
$[Ru(bpy)_3]^{2+}$	10.1×10^4	(6.72×10^4)	99.6×10^4	(7.04×10^4)	150×10^4	(10.6×10^4)
$[Ru(bpy)_2(dmbpy)]^{2+}$	13.6×10^4	(4.54×10^4)	194×10^4	(10.00×10^4)	201×10^4	(10.3×10^4)
dend-4-$Ru(bpy)_3$	12.9×10^4	(5.28×10^4)	91.4×10^4	(4.71×10^4)	105×10^4	(5.43×10^4)
dend-8-$Ru(bpy)_3$	15.7×10^4	(2.56×10^4)	98.7×10^4	(2.42×10^4)	130×10^4	(3.19×10^4)
dend-16-$Ru(bpy)_3$	20.1×10^4	(2.74×10^4)	146×10^4	(3.13×10^4)	182×10^4	(3.90×10^4)
dend-32-$Ru(bpy)_3$	20.8×10^4	(2.84×10^4)	148×10^4	(3.18×10^4)	211×10^4	(4.53×10^4)
dend-64-$Ru(bpy)_3$	11.1×10^4	(1.03×10^4)	80.7×10^4	(58.4×10^4)	115×10^4	(83.5×10^4)

[a] 10% ethanol and 90% butyronitrile. [b] Butyronitrile.

Quantum Yield. The quantum yields for both families of dendrimers were calculated using the total counts of the principal emission peak combined with the known quantum yield of an appropriate reference compound. The two reference compounds used with dend-*n*-$Ru(bpy)_3$ and dend-*n*-$Ru(tpy)_2$ were $[Ru(bpy)_3]^{2+}$ and $[Ru(tpy)_2]^{2+}$, respectively. The values reported in Table 1 are normalized to the effective concentration of chromophores. For $[Ru(tpy)(mtpy)]^{2+}$ and all five generations of dend-*n*-$Ru(tpy)_2$ at 77 K, the quantum yields dropped by about half to approximately 0.23 compared to $[Ru(tpy)_2]^{+2}$ whose reported values is 0.48. The quantum yields of $[Ru(tpy)(mtpy)]^{2+}$ and the dendrimers at 298 K were too small to allow for a precise determination of any changes with generation, but reasoning by analogy, would be expected to be approximately half that for $[Ru(tpy)_2]^{+2}$.

For $[Ru(bpy)_3]^{+2}$, the reported values for the quantum yields at 77 and 298 K are 0.40 and 0.066, respectively.[8] In this case, the d−d metal-centered state is not as readily accessible at room temperature because the geometrical strain present in the $[Ru(tpy)_2]^{+2}$ complex is absent in $[Ru(bpy)_3]^{+2}$. At both temperatures, the change in quantum yield with dendrimer generation follows the same pattern. The quantum yields of $[Ru(bpy)_2(dmbpy)]^{2+}$ and dend-4-$Ru(bpy)_3$ dropped by about 27% to 0.27 at 77 K and 0.049 at 298 K. The values for generations 1−3 were very similar to one another at approximately 0.13 and 0.022 at 77 and 298 K, respectively. The largest dendrimer generation exhibited an anomalously large quantum yield at both temperatures. For example, at 77 K it is 0.48 which exceeds the quantum yield of $[Ru(bpy)_3]^{+2}$. At this time, we are not certain as to the origin of this effect.

Summary of Results. For both families of dendrimers at 77 K, the principal emission peak exhibits a red shift with increasing generation, whereas at 298 K, only a slight red shift was noted. Except in the case of the dend-*n*-$Ru(tpy)_2$ dendrimers at 298 K, the emission lifetime decreased with increasing dendrimer generation. The largest changes in emission lifetimes occurred in the dend-*n*-$Ru(tpy)_2$ dendrimers at low temperature (77 K). The lifetimes of the dend-*n*-$Ru(tpy)_2$ dendrimers in DMAA are longer than in acetonitrile and exhibit a significantly smaller generation dependence. The lifetimes of the dend-*n*-$Ru(bpy)_3$ dendrimers in DMAA are somewhat shorter than in butyronitrile and a similar generation dependence is observed in both solvents.

The changes in the quantum yields of dend-*n*-$Ru(bpy)_3$ dendrimers are very similar at 77 and 298 K. An initial drop was observed for G0 compared to the $[Ru(bpy)_3]^{+2}$ and $[Ru(bpy)_2(dmbpy)]^{2+}$ model compounds. The quantum yield then leveled off for G1-G3, followed by an anomalous increase for G4. The quantum yields of $[Ru(tpy)(mtpy)]^{2+}$ and dend-*n*-$Ru(tpy)_2$ at 77 K were virtually identical ($\phi \approx 0.22$).

Discussion

The photophysical behavior of these families of dendrimers modified with pendant $[Ru(tpy)_2]^{+2}$ and $[Ru(bpy)_3]^{+2}$ chromophores is complex, as evident from the dendrimer-generation dependent variations in the emission wavelengths, the excited state lifetimes, and the solvent dependencies. Some variations in photophysical properties are likely to be related to variations in either the average distance between chromophores or their volume density. We carry out below an analysis of the experimental observations in which we consider Förster and Dexter energy transfer mechanisms and a solvent dependence of the coupling between the emitting MLCT state and (energetically) low-lying metal-centered states.

We begin by considering how the nonradiative decay rates of Ru(II) dendrimer complexes in solution, shown in Table 2, depend on their size or generation number. In short, the experimental finding is that the dependence is quite weak. In the case of the terpyridine complexes, the rate decreases by about 8% from $[Ru(tpy)(mtpy)]^{2+}$ to dend-4-$Ru(tpy)_2$ and then slows by an additional 32% as the size is increased further from dend-4-$Ru(tpy)_2$ to dend-64-$Ru(tpy)_2$. In the case of the bipyridine complexes, the rate increases by about 3% from $[Ru(bpy)_2(dmbpy)]^{2+}$ to dend-4-$Ru(bpy)_3$ and then increases by about 35% from dend-4-$Ru(bpy)_3$ to dend-64-$Ru(bpy)_3$. We will find that the dependence is consistent neither with the dependence of nonradiative processes on size (assuming all vibrational modes to contribute to the nonradiative process) nor with a model in which the decay rate depends on energy transfer between ion centers, assuming either that the ions are uniformly distributed on the surface area or in the volume of the dendrimer. However, the overall magnitude and variation in the emission rates might be explained by a solvent dependence on the coupling between the emitting MCLT state and nearby metal-centered states.

We start with some simple assumptions. Let the number of arms on the dendrimer be $2^n = 4$, 8, 16, 32, or 64, with $n = 2-6$. The generation number, as normally defined, is then $n - 2$. We approximate the length of an arm by a distance parameter, r_o, times n, $L = r_o n$. We may also then approximate the number

of atoms in the dendrimer, N, as the number of arms times the approximate number of atoms per arm, N_o, $N = N_o 2^n$. Finally, the volume and the surface area of the dendrimer complex may be approximated as respectively $(4/3)\pi$ times the cube of the length of an arm, $V = (4/3) = (r_o n)^3$, and 4π times the square of the length of an arm, $A = 4 = (r_o n)^2$. Because there is evidence from molecular dynamics simulations that these simple formulas do not reproduce the volume and surface area of the dendrimer, we will also consider the values derived from these simulations, namely, radii of 29, 32.5, 35, 42.5, and 50 Å for $n = 2-6$, respectively. With these approximations, the Appendix examines a number of physical processes that can govern the lifetime of the emission. We summarize these results here.

One mechanism to consider is the effect of vibrational coupling on the nonradiative decay rate. In this model, the emission decay rate would be governed by the coupling between the MLCT state and the ground state of the dendrimer−ruthenium complex. If all of the vibrational modes were to contribute to the nonradiative decay, then as the number of modes increases with increasing generation number the density of states will increase dramatically and cause a rather drastic initial increase in k_{nr}. The predicted increase is far larger than observed experimentally (details are provided in the Appendix), so we conclude that only a few modes contribute to the nonradiative decay and that this number does not change substantially with generation. See Table 2 for the experimental values of k_{nr}. Nonradiative decay via vibrational coupling is thus not likely to be the cause of the observed changes in the nonradiative decay rate.

Another mechanism to consider concerns the proximity of the metal centers. In this model, one might imagine that the environment of a particular metal center might be more favorable for relaxation of the MCLT state and that energy would be exchanged between the metal centers on a particular dendrimer until it is "trapped" by relaxation at the favorable site. Either the Förster[34] or Dexter[35−37] mechanism could, in principle, control the energy transfer. A similar idea has been considered by Barigelletti et al. for excitation transfer between Ru(II) and Os(II) terpyridine complexes.[30] In the case of Förster transfer, the rate should go as $k \propto r^{-6}$, where r is the distance between centers, whereas in the case of Dexter transfer, the rate is described as a double exchange of electrons between donor and acceptor and is related to the free energy change, $\Delta G^{\ddagger}$, for the process. Because of the requirement for overlap of wave functions, the Dexter transfer decreases exponentially with distance. Both Förster and Dexter mechanisms are considered in detail in the Appendix, where it is shown that neither fits the generation dependence data.

A final model for the change in emission decay rate with generation number involves solvent shifts of the relative energies between the ^{3}MC and ^{3}MLCT states. Scheme 1 provides a schematic energy level diagram. Indelli et al. noted a strong solvent shift in both the emission maximum and the lifetime of $[Ru(tpy)(CN)_3]^-$ in solvents of acceptor number ranging from acetone to water.[38] Longer lifetimes (lower emission rate constants) were associated with an increasing red shift of the emission. Although this general correlation likely holds for $[Ru(tpy)_2]^{2+}$, $[Ru(tpy)(mtpy)]^{2+}$, and the terpyridine dendrimers studied here, it is not observed for $[Ru(bpy)_3]^{+2}$, $[Ru(bpy)_2(dmbpy)]^{+2}$, and the bipyridine dendrimers. A possible explanation for the difference between the terpyridine and bipyridine complexes is that, in the former, there is substantial competition between emission from the ^{3}MCLT state and that from the ^{3}MC state to which it is thermally coupled (and which decays rapidly with $k_{nr}^{MC} \gg k_{nr}^{MLCT}$), whereas in the latter, this competition is diminished by the much larger energy separation between the two states.[8] Thus, one might expect solvent changes to affect the rate of emission decay of terpyridine complexes by changing the ratio between k_f and k_r, whereas what little effect they would have for the bipyridine complexes would come from solvent effects on k_{nr}^{MLCT}. One model for the monotonic decrease in emission rate in going from the dend-4 to dend-64 terpyridine complexes is to assume that the replacement of a tpy group in $[Ru(tpy)_2]^{+2}$ by the dend-4-$Ru(tpy)_2$ shifts both the ^{3}MCLT and ^{3}MC states in such a way as to make the emission rate increase slightly. Thereafter, an increase in the size of the dendrimer amounts to a monotonic solvation change in the energy difference between these two states. The Appendix suggests that the dendrimer itself would solvate the metal complex so as to increase the energy difference and decrease the rate. Assuming a low rate for the dendrimer and a rapid rate for acetonitrile, the data may be fit by considering how the dendrimer replaces the acetonitrile as the size of the dendrimer is increased.

The difference in solvent dependence between dend-n-$Ru(bpy)_3$ and dend-n-$Ru(tpy)_2$ suggests that for the dend-n-$Ru(bpy)_3$ species the chromophores are less sensitive to the dendritic backbone than in dend-n-$Ru(tpy)_2$. In retrospect, this is not a surprising result because, in the former, two of the coordinating centers (i.e., one bipyridine) are part of the dendritic backbone, whereas in the latter, there are three (one terpyridine). Another key difference to be considered is the extreme difference in the excited state lifetimes in the two cases. For example, the lifetimes of the bpy materials are sufficiently long that molecular diffusion rates could contribute a collisional deactivation decay pathway. A third possibility related to the difference in lifetime is electron delocalization. Although it is well-known that the excited-state electron in $[Ru(bpy)_3]^{+2}$ is localized on a single ligand, McCusker et al. have used femtosecond time-resolved absorption anisotropy to look at early times of the excited state and found that the electron is initially delocalized.[39] The lifetime of the tpy materials could be short enough to reflect the induced symmetry and related solvent response of a delocalized electron. An indication that more than one mechanism is at work is that, for the tpy materials, the lifetime gets longer with increasing generation, whereas the opposite trend is found for the bpy materials at room temperature.

There are other observations that lend further support to the idea that the solvent plays an important, if not key, role in the relaxation dynamics. As mentioned earlier, in acetonitrile at 298 K, the change in the experimental lifetimes of the dend-n-$Ru(tpy)_2$ dendrimers gets longer with increasing dendrimer generation. However, such changes were much less pronounced when using DMAA as the solvent. This suggests that the dendritic arms play a significant role in defining the solvent sphere surrounding each chromophore. The fact that the differences observed in acetonitrile are greatly attenuated in DMAA is consistent with experimental observation as is the previously mentioned study of the kinetics of electron transfer of adsorbed layers of dend-64-$[Ru(tpy)_2]$. Thus far, we conclude that solvent effects on the coupling between the ^{3}MLCT and ^{3}MC states could explain the observed decay rates.

Conclusions

The photophysics of generations 0−4 of poly-amidoamine based dendrimers modified with (4, 8, 16, 32, and 64) pendant-$[Ru(tpy)_2]^{+2}$ and $[Ru(bpy)_3]^{+2}$ chromophores on the periphery have been studied in both fluid solution at 298 K and frozen

glass at 77 K media. The absorption and emission spectra, the excited-state lifetimes, and the quantum yields have been obtained for both families of metallodendrimers. The behavior of these metallodendrimers parallels that exhibited by discrete molecular analogues (i.e., $[Ru(tpy)_2]^{+2}$ and $[Ru(bpy)_3]^{+2}$) with the bipyridine derivatives exhibiting longer lifetimes and higher quantum yields when compared to the corresponding terpyridine complexes. Some generation dependent variations have also been observed. Of particular note, the low temperature excited state lifetime for the terpyridine dendrimers, decreased linearly with the cube root of the molecular weight (and thus the dendrimers size), which would suggest an effect of the proximity of adjacent chromophores. We have also explored the effects of solvent by comparing results in butyronitrile and dimethylacetamide with the latter being used as a mimic of the dendritic backbone. These results suggest that, for the higher generations, the dendritic backbone acts as the solvent in affecting the photophysical behavior.

Acknowledgment. This work was supported by the Cornell Center for Materials Research (CCMR), a Materials Research Science and Engineering Center of the National Science Foundation (DMR-9632275). We are grateful to Debra Collier, supported by the REU program of the CCMR, for collecting the emission spectra reported in this work. The help of Dr. Heikel in data fitting and analysis is gratefully acknowledged.

Appendix

In this appendix, we consider a number of physical processes that can govern the lifetime of MLCT emission.

Nonradiative Processes. Nonradiative decay is governed by the number of vibrational modes of the lower electronic state that can couple to the electronically excited state. We thus need to know the density of vibrational levels. In the classical limit, the density of states $\tilde{n}(E)$ is given by the formula[40]

$$\rho(E) = \frac{E^{s-1}}{(s-1)!\prod h\nu_i} \tag{A1}$$

The "Golden Rule" then gives the rate of intramolecular relaxation in the statistical limit as a line width, $\tilde{A}_{ER}$

$$\Gamma_{ER} = \frac{2\pi}{\hbar}\langle n|v|f\rangle\rho_f \tag{A2}$$

setting the line width $\tilde{A}$ equal to the nonradiative decay rate k_{nr}, setting s, the number of oscillators, equal to $3N - 1$, and finally neglecting small integers with respect to $3N$ gives

$$k_{nr}\frac{E^{3N}}{(3N)!\prod^{3N} h\nu_i} \approx \frac{E^{3N}}{(3N)!(h\nu_{av})^{3N}} \tag{A3}$$

or

$$\ln k_{nr} = \ln C + (3N)\ln(E/(h\nu_{av})) - \ln(3N)! \tag{A4}$$

where ν_{av} is the geometric mean of the vibrational frequencies $[\Pi h\nu_i = (h\nu_{av})^{3N}]$ and C is a constant. Using Stirling's approximation for ln $(3N)!$, we find that

$$\ln k_{nr} = \ln C + (3N)\{\ln(E/(h\nu_{av})) - \ln(3N) + 1\} \tag{A5}$$

Because $E/(h\nu_{av})$ is a fairly large number (about 20 000 cm^{-1}/50 cm^{-1}, or 400) and because this number does not vary strongly with N, k_{nr} will increase with increasing size until $3N \approx E/h\nu_{av}$ and then decrease. A detailed investigation of this formula shows that if all of the modes were to contribute to the nonradiative decay increasing the generation by one would more than double $3N$ and cause a rather drastic initial increase in k_{nr}. Thus, we conclude that only a few modes contribute to the nonradiative decay and that this number does not change substantially with generation. Nonradiative decay is not likely to be the cause of the observed nearly monotonic decrease in the nonradiative rate with increasing generation number.

Proximity of Metal Ions. Another possibility we considered is that the decay rate might depend on the distance between the excited MLCT moiety and an adjacent unexcited one. There are two ways to view this. First, suppose that all of the metal ions are on the surface of the (spherical) dendrimer molecule. The surface area, $A = 4\pi(r_0 n)^2$, is proportional to n^2. The number of metal ions is the number of arms, 2^n, so the area on the surface of the sphere occupied by each metal ion is proportional to $n^2/2^n$. The distance between each metal ion would then scale as the square root of this area, or as $n/2^{n/2}$. For either Förster or Dexter decay mechanisms, the rate of emission falls very strongly with distance, much more strongly than the data if the distance is given by the above simple formula for ions on the surface of a sphere.

On the other hand, it is possible that the metal ions are within the volume of a sphere, $V = (4/3)\pi(r_0 n)^3$, rather than on its surface. Because the volume scales as n^3, the volume per ion scales as $n^3/2^n$, the radius of an ion within the volume would then vary as the cube root of $(n^3/2^n)$. Again, either Förster or Dexter energy transfer would predict a much larger variation with distance than we observe. We conclude that the data is not consistent with models in which the decay rate depends on the distance between metal centers if this distance is calculated from the simple formula given above.

Instead of using dendrimer radii obtained from these simple formulas, we next consider using those obtained from molecular modeling. Then, either for the metal centers on the surface of a sphere or within the volume of the sphere, it is easy to calculate that the distance between centers *decreases* with generation number, indicating that the rate should *increase*, in contrast to the room-temperature data for the $[Ru(tpy)_2]^{2+}$ complexes. The trend, though not the magnitude, does agree with the low-temperature data. One can thus rule out either Förster or Dexter transfer in this hypothesis for the measurements at room temperature. Ghiggino et al. used time-resolved fluorescence anisotropy measurements in a rigid glass to probe the electronic energy transfer in three generations ($n = 4$, 16, and 64) of porphyrin functionalized dendrimers and found that the Förster mechanism adequately predicted the results for G0 but not for the larger generations.[41] Perylene-terminated monodendrons were found by Moore et al. to exhibit an energy gradient from the periphery to the core, but the energy transfer process could not be explained by the Förster mechanism.[42] Although the reasons that the Förster mechanism has not proven useful in the analysis of photophysical data of starburst dendrimers are specific to the system under study, very little evidence exists supporting energy transfer between chromophores in dendrimers. In our dendrimers, the overlap between the absorption and emission spectra for both of the ruthenium polypryridyl complexes is small, and the Förster mechanism is dependent on overlap between the absorption spectrum of the acceptor and the emission spectra of the donor. So, it is not surprising that there is only phenomenological evidence of energy transfer between ruthenium centers. Of particular note, the low temper-

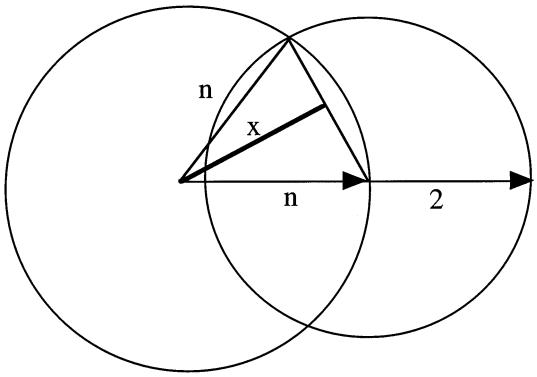

Figure 6. Intersection volume of two spheres. Distances are in units of r_0. The sphere on the right is the sphere in which the presence of solvent can affect the decay rate of a metal ion located at its center. The metal ion is assumed to be on the surface of the sphere on the left, of radius nr_0. The volume of overlap of the two spheres represents the volume of solvent excluded by the dendrimer.

ature excited state lifetime for the terpyridine dendrimers decreased linearly with the cube root of the molecular weight (and thus size), which would suggest an effect of the proximity of adjacent chromophores.

It should also be mentioned that analysis of the absorption spectra for both dendrimer families and model compounds, including ligand based as well as MLCT processes, point to the absence of any significant interactions. Plots of the molar absorptivity calculated from absorption spectra, as a function of the number of chromophores, exhibited an excellent linear correlation with R^2 values on the order of 0.99. This linear relationship also indicates that each dendrimer generation is fully substituted with 4, 8, 16, 32, or 64 pendant groups. Further evidence of the isolated nature of the peripheral chromophores is given by the fact that (except for dend-64-Ru(bpy)$_3$) the quantum yield did not vary appreciably with dendrimer generation. If intramolecular energy transfer were occurring by the Förster mechanism, the quantum yield would decrease with increasing dendrimer generation, because the metal-to-metal distance would become shorter and assuming that any subsequent emission would occur at a slightly red shifted wavelength.

Solvent Effects. The key idea behind this model is that the variation in decay rate is due to the solvation of the metal ion and that the amount of solvent available is a function of the size of the dendrimer; the larger the dendrimer, the less solvent is available near the excited metal ion. The model does require, however, assignment of one parameter: the distance over which the solvent matters. Let us choose this distance to be the diameter of the $n = 3$ dendrimer, which is twice the arm length or $2L = 2r_0n = 6r_0$, because $n = 3$. Thus, we need to see how much solvent vs dendrimer is in the volume $(4/3)\pi(6r_0)^3$. The volume of the dendrimer for $n = 3$ is $(4/3)\pi(3r_0)^3$, and all of this is within the volume over which the solvent is effective. The ratio of dendrimer to total volume is thus $3^3/6^3 = 1/8$. If the dendrimer were infinitely large, then, assuming the metal ion to be in the center of the solvent sphere, the dendrimer would fill half of the volume over which the solvent is effective. Thus, the amount of nondendrimer solvent drops from 7/8 to 1/2 as n goes from 3 to infinity. We then assume that the decay rate is proportional to the amount of solvent available, so that it decreases with dendrimer size. To calculate how this decrease depends on the generation number, we need to know the volume of intersection of two spheres of different radii, where, as shown in Figure 6, the outer surface of one sphere (the dendrimer, of radius nr_0) goes through the center of the other sphere (the sphere of radius $6r_0$ representing the volume of solvent that matters).

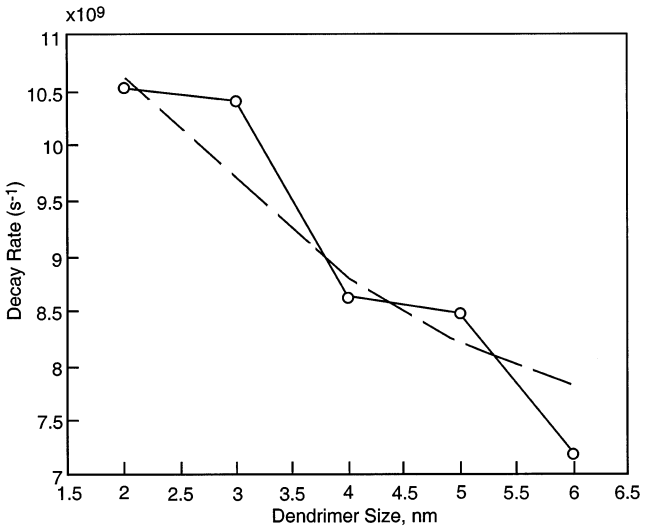

Figure 7. Open circles connected by solid lines which represent the measured room-temperature decay rates for ruthenium dendrimers (dend-#-(tpy)$_2$) as a function of generation number. The dashed line gives the prediction of a model in which the relaxation depends on the amount of solvent excluded by the size of the dendrimer from the vicinity of the excited ion center.

The solvent sphere is centered on the excited metal ion. When $n \leq 3$, the dendrimer sphere is entirely within the solvent sphere, so the amount of solvent available in the effective region is just proportional to the difference in volumes. For larger dendrimers, as shown in the figure, the volume of excluded solvent is the volume of intersection of the two spheres and may be determined by calculating the sum of the volumes of two polar caps, one for each sphere. The length x is given by $(n^2 - 3^2)$. Note also that $\sin(\theta) = x/n$. The area of a sphere from a polar angle of $\theta = 0$ to one of angle θ is given by πr_0^3 times the integral from 0 to θ of $\sin^3\theta\, d\theta$. The polar cap for the right-hand sphere that contributes to the intersection volume is the integral from a polar angle of $\theta = 0$ down to a polar angle of θ. The polar cap for the left-hand sphere is the integral from a polar angle of $\theta = 0$ down to an angle given by twice $90 - \theta$. The intersection area is the sum of these two integrals. The resulting fraction of the effective volume occupied by solvent is found to be 0.96, 0.88, 0.78, 0.73, and 0.68 for $n =$ 2, 3, 4, 5, and 6, respectively.

Given these solvent volumes, we can model the relaxation rates of the dendrimers by assuming something about the way that the dendrimer itself solvates the metal center. The data for DMMA show that, even for this solvent more closely resembling the backbone of the dendrimer, the rate still decreases with increasing dendrimer size. If we say that the dendrimer itself as a solvent relaxes the metal center with a relaxation rate of approximately $1 \times 10^9\ s^{-1}$ (somewhat lower than DMMA) and that the acetonitrile solvates the metal center with a larger relaxation rate or about $1.1 \times 10^{10}\ s^{-1}$, then we find that the sum of these rates weighted by the fraction of the effective volume that corresponds to the dendrimer gives more or less what is observed for the different dendrimer generations. In Figure 7, the data are the points connected by the solid line with the prediction. We conclude that it is quite possible that the observed variation of relaxation rate with generation number is due to the fact that the solvent is excluded from the vicinity of the metal ion as the dendrimer size increases.

References and Notes

(1) Sauvage, J.-P.; Collin, J.-P.; Chambron, J.-C.; Guillerez, S.; Coudret, C. *Chem. Rev.* **1994**, *94*, 993.

(2) Stone, M. L.; Crosby, G. A. *Chem. Phys. Lett.* **1981**, *79*, 169.

(3) Creutz, C.; Chou, M.; Netzel, T. L.; Okumura, M.; Sutin, N. *J. Am. Chem. Soc.* **1980**, *102*, 1309.

(4) Winkler, J. R.; Netzel, T. L.; Creutz, C.; Sutin, N. *J. Am. Chem. Soc.* **1987**, *109*, 2381.

(5) Demas, J. N.; DeGraff, B. A. *Anal. Chem.* **1991**, *63*, 829.

(6) Nakamaru, K. *Bull. Chem. Soc. Jpan.* **1982**, *55*, 2697.

(7) Meyer, T. J. *Acc. Chem. Res.* **1989**, *22*, 163.

(8) Kalyanasundaram, K. Polypyridyl Complexes of Ru, Os and Fe. In *Photochemistry of Polypridine and Porphyrin Complexes*; Academic Press: San Diego, 1992; p 105.

(9) Balzani, V.; Scandola, S. *Supramolecular Photochemistry*; Horwood: Chichester, U.K., 1991.

(10) Lehn, J. M. *Supramolecular Chemistry, Concepts and Perspectives*; VCH: New York, 1995.

(11) Wasielewski, M. R. *Chem. Rev.* **1992**, *92*, 435.

(12) Owen, A.; Shipway, A. N.; Stoddart, J. F. *Prog. Polym. Sci.* **1998**, *23*, 1.

(13) Philp, D.; Stoddart, J. F. *Angew. Chem., Int. Ed. Engl.* **1996**, *35*, 1154.

(14) Tomalia, D. A. *Adv. Mater.* **1994**, *6*, 529.

(15) Newkome, G. R.; Morrefield, C. N.; Vogtle, F. *Dendritic Molecules: Concepts, Syntheses, Perspectives*; VCH: Weinheim, Germany, 1996.

(16) Zeng, F.; Zimmerman, S. C. *Chem. Rev.* **1997**, *97*, 1681.

(17) Moore, J. S. *Acc. Chem. Res.* **1997**, *30*, 402.

(18) Mathews, O. A.; Shipway, A. N.; Stoddart, J. F. *Prog. Polym. Sci.* **1998**, *23*, 1.

(19) Frey, H.; Lach, C.; Lorenz, K. *Adv. Mater.* **1998**, *10*, 279.

(20) Gorman, C. *Adv. Mater.* **1998**, *10*, 295.

(21) Tomalia, D. A.; Naylor, A. M.; III, W. A. G. *Angew. Chem., Int. Ed. Engl.* **1990**, *29*, 138.

(22) Fréchet, J. M. J. *Science* **1994**, *263*, 1710.

(23) Storrier, G. D.; Takada, K.; Abruña, H. D. *Langmuir* **1999**, *15*, 872.

(24) Bradley, P. G.; Kress, N.; Hornberger, B. A.; Dallinger, R. F.; Woodruff, W. H. *J. Am. Chem. Soc.* **1981**, *103*, 7441.

(25) Klassen, D. M.; Crosby, G. A. *J. Chem. Phys.* **1968**, *48*, 1853.

(26) Takada, K.; Storrier, G. D.; Morán, M.; Abruña, H. D. *Langmuir* **1999**, *15*, 7333.

(27) Nakamaru, K. *Bull. Chem. Soc. Jpan.* **1982**, *55*, 1639.

(28) Hecht, S.; Vladimirov, N.; Frechet, J. M. J. *J. Am. Chem. Soc.* **2001**, *123*, 18.

(29) Caspar, J. V.; Meyer, T. J. *J. Am. Chem. Soc.* **1983**, *105*, 5583.

(30) Barigelletti, F.; Belser, P.; Zelewsky, A. V.; Juris, A.; Balzani, V. *J. Phys. Chem.* **1985**, *89*, 3680.

(31) Amatore, C.; Bouret, Y.; Maisonhaute, E.; Goldsmith, J. I.; Abruña, H. D. *ChemPhysChem* **2001**, *2*, 130.

(32) Amatore, C.; Bouret, Y.; Maisonhaute, E.; Goldsmith, J. I.; Abruña, H. D. *Chem. Eur. J.* **2001**, *7*, 2206.

(33) Reitz, G. A.; Demas, J. N.; DeGraff, B. A.; M., S. E. *J. Am. Chem. Soc.* **1988**, *110*, 5051.

(34) Förster, T. *10th Spiers Memorial Lecture* **1959**, 7.

(35) Dexter, D. L. *J. Chem. Phys.* **1953**, *21*, 836.

(36) Scandola, F.; Balzani, V. *J. Chem. Educ.* **1983**, *60*, 814.

(37) Closs, G. L.; Miller, J. R. *Science* **1988**, *240*, 440.

(38) Indelli, M. T.; Bignozzi, C. A.; Scandola, F. *Inorg. Chem.* **1998**, *37*, 6084.

(39) Yeh, A. T.; Shank, C. V.; McCusker, J. K. *Science* **2000**, *289*, 935.

(40) Baer, T. *Unimolecular Reaction Dynamics, Theory and Experiment*; Oxford U. Press: New York, 1996.

(41) Yeow, E. K. L.; Ghiggino, K. P.; Reek, J. N. H.; Crossley, M. J.; Bosman, A. W.; Schenning, A. P. H. J.; Meijer, E. W. *J. Phys. Chem. B* **2000**, *104*, 2596.

(42) Devadoss, C.; Bharathi, P.; Moore, J. S. *J. Am. Chem. Soc.* **1996**, *118*, 9635.